PROTEINS: Structure, Function, and Bioinformatics 68:337–343 (2007)

Structural and Kinetic Analysis of Proton Shuttle Residues in the Active Site of Human Carbonic Anhydrase III

Ileana Elder,[1] Zoë Fisher,[2] Philip J. Laipis,[2] Chingkuang Tu,[1] Robert McKenna,[2]* and David N. Silverman[1,2]*
[1]*Department of Pharmacology and Therapeutics, University of Florida College of Medicine, Gainesville, Florida 32610-0267*
[2]*Department of Biochemistry and Molecular Biology, University of Florida College of Medicine, Gainesville, Florida 32610*

ABSTRACT **We report the X-ray crystal structures and rate constants for proton transfer in site-specific mutants of human carbonic anhydrase III (HCA III) that place a histidine residue in the active-site cavity: K64H, R67H, and K64H-R67N HCA III. Prior evidence from the exchange of ^{18}O between CO_2 and water measured by mass spectrometry shows each mutant to have enhanced proton transfer in catalysis compared with wild-type HCA III. However, His64 in K64H and K64H-R67N HCA III have at most a capacity for proton transfer that is only 13% that of His64 in HCA II. This reduced rate in mutants of HCA III is associated with a constrained side-chain conformation of His64, which is oriented outward, away from the active-site zinc in the crystal structures. This conformation appears stabilized by a prominent π stacking interaction of the imidazole ring of His64 with the indole ring of Trp5 in mutants of HCA III. This single orientation of His64 in K64H HCA III predominates also in a double mutant K64H-R67N HCA III, indicating that the positive charge of Arg67 does not influence the observed conformation of His64 in the crystal structure. Hence, the structures and catalytic activity of these mutants of HCA III containing His64 account only in small part for the lower activity of this isozyme compared with HCA II. His67 in R67H HCA III was also shown to be a proton shuttle residue, having a capacity for proton transfer that was approximately four times that of His64 in K64H HCA III. This is most likely due to its proximity and orientation inward towards the zinc-bound solvent. These results emphasize the significance of side chain orientation and range of available conformational states as characteristics of an efficient proton shuttle in carbonic anhydrase. Proteins 2007;68:337–343.** © 2007 Wiley-Liss, Inc.

Key words: carbonic anhydrase; proton transfer; oxygen-18; histidine; isotope exchange

INTRODUCTION

Human carbonic anhydrase III (HCA III) is the least catalytically efficient of the carbonic anhydrases in the α-class with k_{cat} near 3 ms^{-1},[1] while HCA II is among the most efficient with k_{cat} near 10^3 ms^{-1}.[2] HCA II and HCA III have a sequence identity of 60% with backbone atoms closely superimposable,[3,4] as was also observed for the bovine enzymes.[5] The catalytic pathway of these enzymes occurs in two distinct and separate stages: the interconversion of carbon dioxide and bicarbonate [Eq. (1)] followed by proton transfer steps that regenerate the zinc bound hydroxide for the next round of catalysis [Eq. (2)].[6,7]

$$CO_2 + EZnOH^- \leftrightharpoons EZnHCO_3^- \overset{H_2O}{\leftrightharpoons} EZnH_2O + HCO_3^- \quad (1)$$

$$EZnH_2O + B \leftrightharpoons EZnOH^- + BH^+ \quad (2)$$

Here B is a proton acceptor that may be an exogenous general base or a residue of the enzyme itself that transports the proton to solution. In catalysis of the hydration of CO_2 by HCA II, B is the proton shuttle residue His64.[8,9] Structural and kinetic studies of catalysis by HCA II have been helpful in explaining the role of the side chain of His64 in transporting protons between the active site and bulk solution.[6,8–10] In contrast to the catalytically efficient HCA II, HCA III has a lysine at position 64, which is an inefficient proton shuttle in part because it is too basic.[1,5,11] In addition, crystal structures of bovine, rat, and human CA III show the side chain of Lys64 pointing out of the active-site cavity away from the zinc (Fig. 1).[3,5,14] Two other residues that are thought to adversely affect catalysis in the active site of HCA III are Arg67 (Asn67 in HCA II) and Phe198 (Leu198 in HCA II).[3,11,15,16]

In this study, we report the crystal structures of mutants K64H, R67H, and the double mutant K64H-R67N HCA III, and compare them with wild-type HCA II and III, to understand specific properties of the proton

Abbreviations: HCA III, human carbonic anhydrase III; K64H HCA III, the mutant of human carbonic anhydrase III with Lys64 replaced with His; 4-MI, 4-methylimidazole.

Grant sponsor: Maren Foundation; Grant sponsor: NIH; Grant number: GM 25154.

Ileana Elder and Zoë Fisher contributed equally to this work.

*Correspondence to: D. N. Silverman, Box 100267 Health Center, University of Florida, Gainesville, FL 32610-0267. E-mail: silvermn@college.med.ufl.edu or R. McKenna, Box 100245 Health Center, University of Florida, Gainesville, FL 32610-0245. E-mail: rmckenna@ufl.edu

Received 7 July 2006; Revised 21 October 2006; Accepted 27 December 2006

Published online 11 April 2007 in Wiley InterScience (www.interscience.wiley.com). DOI: 10.1002/prot.21403

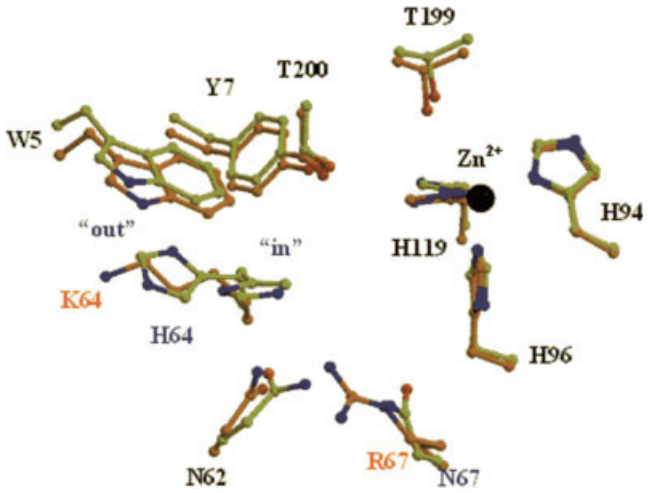

Fig. 1. Active site comparison of wild type HCA II[4] and III.[3] Superposition of wild type HCA II (yellow) and HCA III (orange) active sites. The zinc atom is shown as a black sphere and the active site residues are in ball-and-stick as labeled. Residues that are invariant between the two isozymes are labeled in black. Residues that differ between HCA II and III are labeled in blue and orange, respectively. Figure was generated with Bobscript and rendered with Raster3D.[12,13]

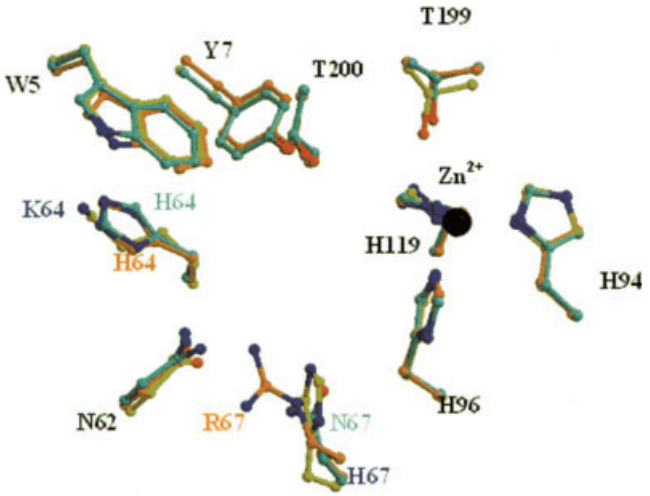

Fig. 2. Active site comparison of HCA III K64H, R67H, and K64H/R67N. Superposition of HCA III K64H (orange), R67H (yellow), and K64H-R67N (cyan) active sites. The zinc atom is shown as a black sphere and active site residues are in ball-and-stick as labeled. Residues that are invariant between HCA III mutants are labeled in black. Residues differing between K64H, R67H, K64H-R67N are labeled in orange, blue, and cyan, respectively. This figure was generated with Bobscript and rendered with Raster3D.[12,13]

shuttle residues in carbonic anhydrase. These structural studies address how the active-site environment of carbonic anhydrase affects the conformation and proton shuttle capacity of histidine residues. Analysis of these structures suggests that the imidazole side chain of His64 in K64H and K64H-R67N HCA III adopts a limited conformational state with the imidazole side chain oriented away from the zinc and pointing out toward solution. These data support earlier findings that demonstrate an association between low activity in variants of carbonic anhydrase and an outward orientation of His64 in the crystal structure.[17] These studies show that the constraints on the side chain conformations of His64 imposed by the nearby side chain of Trp 5 appear more significant than that imposed by Arg67 which extends into the active-site cavity. The enhancement of the proton transfer rate observed for His 67 in R67H HCA III, compared to HCA III, appears to be associated with the proximity and orientation of the side chain with respect to the zinc-bound solvent. These results emphasize the significance of side chain orientation in efficient proton transfer in carbonic anhydrase.

MATERIALS AND METHODS

Enzymes

Expression vectors containing the coding region for the single mutants K64H and R67H HCA III, and for double mutants K64H-R67N and K64A-R67H HCA III (all mutated by site-directed mutagenesis),[18] were expressed by transforming into *Escherichia coli* BL21(DE3)pLysS.[19] The coding vectors for these mutants contained the replacement of two cysteine (Cys 182 and Cys188) residues located at the surface of the protein to serines. This replacement greatly enhanced crystallization perhaps by avoiding oxidation of the thiol side chains of the Cys residues. The vector sequence for the R67H HCA III mutant used for crystallization contained an additional mutation of Pro replaced by Arg at position 42 (P42R). Residue 42 is located at the surface of HCA III with the side chain extending into solution on the backside opposite to the active site and is not involved in catalysis. This was confirmed by comparison of the recombinant HCA III with HCA III obtained from human muscle (1). Data acquisition and analysis proceeded with this mutant and will be referred to as R67H HCA III in the text. The sequence of each mutant was confirmed by sequencing the DNA of the entire coding region. All mutated HCA III proteins were purified by gel filtration and ion exchange chromatography.[20] Enzyme concentrations were determined from the molar absorptivity at 280 nm of HCA III ($6.2 \times 10^4\ M^{-1}\text{cm}^{-1}$). The purity of enzyme samples was verified by electrophoresis on a 10% polyacrylamide gel stained with Coomassie.

Catalysis

The exchange of ^{18}O between CO_2 and water at chemical equilibrium, both uncatalyzed and catalyzed by carbonic anhydrase, were measured in the absence of buffer at a total substrate concentration of 25–100 mM using membrane-inlet mass spectrometry.[21] The reaction solution is in contact with a membrane permeable to gases, CO_2 passing across the membrane enters a mass spectrometer (Extrel EXM-200) providing a continuous measure of isotopic content of CO_2. The temperature was 25°C and the total ionic strength of solution was kept at

TABLE I. X-Ray Crystallographic Structure Statistics for K64H, R67H, and K64H-R67N HCA III

	K64H	R67H	K64H-R67N
Data Collection			
Resolution (Å)	20.0–1.7 (1.76–1.70)*	20.0–2.6 (2.69–2.60)*	20.0–2.5 (2.59–2.50)*
Space group	$P2_12_12_1$	$P2_12_12_1$	$P2_12_12_1$
Unit cell (Å)	$a = 41.8$, $b = 50.8$, $c = 117.9$	$a = 80.2$, $b = 78.1$, $c = 43.4$	$a = 42.4$, $b = 51.7$, $c = 117.7$
Molecules (AU)	1	1	1
R_{sym} (%)[a]	6.3 (35.7)	9.6 (28.6)	10.4 (37.0)
Reflections (unique)	27406 (2481)	8326 (782)	8529 (809)
Completeness (%)	96.4 (89.0)	94.2 (90.8)	90.3 (88.5)
Refinement			
Residue built	2–261	5–261	4–261
Water molecules	306	50	35
Average B factors (Å^2)			
Protein main-chain	14.6	23.2	38.2
Protein side-chain	16.1	23.8	38.8
Solvent molecules	24.8	23.5	36.8
R_{cryst}/R_{free} (%)[b]	20.5/21.9	18.9/21.7	20.4/23.9
R.m.s.d bond lengths (Å)/angles (°)[c]	0.005/1.3	0.006/1.3	0.007/1.4

*Data for the highest resolution shell are given in parentheses.
[a]$R_{sym} = \Sigma|I - \langle I\rangle|/\Sigma I \times 100$, where I is the intensity of a reflection and $\langle I\rangle$ is the average intensity.
[b]$R_{cryst} = \Sigma_{hkl}|F_0 - KF_c|/\Sigma_{hkl}|F_0| \times 100$, R_{free} is calculated from 5% randomly selected data for cross-validation.
[c]R.m.s.d., root mean square deviation.

a minimum of 0.2M by the addition of Na_2SO_4. This method measures the rate of depletion of ^{18}O from CO_2 and the rate of release of $H_2{}^{18}O$ from the enzyme [Eqs. (3) and (4)].[21]

$$HCOO^{18}O^- + EZnH_2O \leftrightharpoons EZnHCOO^{18}O^- \leftrightharpoons COO + EZn^{18}OH^- \quad (3)$$

$$EZn^{18}OH^- + BH^+ \leftrightharpoons EZnH_2{}^{18}O + B \overset{+H_2O}{\leftrightharpoons} EZnH_2O + H_2{}^{18}O + B \quad (4)$$

Two rates at chemical equilibrium can be determined from this exchange[21,22]: R_1 is the rate of interconversion of CO_2 and HCO_3^- [Eq. (3)]; R_{H_2O}, is a rate of proton transfer to the transitory ^{18}O label at the active site of carbonic anhydrase [Eq. (4)].

The value of R_{H_2O} can be interpreted in terms of the rate constant from an exogenous donor group to the zinc-bound hydroxide according to Eq. (5), in which k_B is the rate constant for proton transfer to the zinc-bound hydroxide, $(K_a)_{donor}$ is the ionization constant of the donor group and $(K_a)_{ZnH_2O}$ is the ionization constant of the noninteracting zinc-bound water molecule. The determination of kinetic constants k_B from Eq. (5) was carried out by nonlinear least-squares methods (Enzfitter, Biosoft).

$$R_{H_2O}/[E] = k_B/\{(1 + (K_a)_{donor}/[H^+])(1 + [H^+]/(K_a)_{ZnH_2O})\} \quad (5)$$

Crystallography

Crystals of K64H, R67H, and K64H-R67N HCA III were grown by hanging drop vapor diffusion.[23] A drop of enzyme solution was prepared by mixing 5 μL of 10 mg/mL protein solution with 5 μL of reservoir solution (0.2M ammonium acetate, 0.1M sodium acetate, and 30% (w/v) polyethylene glycol 4000 at a final pH of 5.8). The drop equilibrated by vapor diffusion over a well containing 0.5–1.0 mL of reservoir solution at 277 K. Crystals appeared within 7–10 days.

X-ray diffraction data were collected using a Rigaku HU-H3R CU rotating anode generator operating at 50 kV and 100 mA, fitted with Osmic mirrors, a 0.3 mm collimator, and a R-AXIS IV^{++} image-plate (IP) system. A total of 120° of data were collected from a single K64H HCA III crystal at 277 K with a crystal to IP distance of 120 mm and exposure time of 300 s/1° frame. The R67H HCA III crystals were more sensitive to radiation damage and three crystals were used for data collection at 277 K for a total of 80° of data using the same optical bench set up as for the K64H HCA III crystal. A single crystal of K64H-R67N HCA III was used for 100° of data with a crystal to IP distance of 150 mm and an exposure time of 420 s/1° frame. All data sets were indexed and processed with the programs DENZO and SCALEPACK.[24] Data set statistics for all three structures are shown in Table I.

The structures of K64H and R67H HCA III were determined by molecular replacement using the structure of wild type HCA III[3] with software package CNS.[25] This structure had residues 64 and 67 mutated to alanines and contained no zinc or solvent to negate the possibilities of model phase bias. A cross-rotation function of the K64H HCA III data with HCA III, resulted in a single solution with $\theta_1 = 12.40$, $\theta_2 = 51.11$, $\theta_3 = 19.34°$, and a peak of 4.2σ above the mean, and subsequent translation function translation components $T_x = 4.55$, $T_y =$

15.18, $T_z = 51.75$ Å, and a correlation coefficient of 0.53. Rigid-body refinement at 20.0–1.7 Å resolution resulted in an initial R_{work} of 0.43. Similarly, a cross-rotation function of the R67H HCA III data resulted in a single solution with $\theta_1 = 349.21$, $\theta_2 = 76.37$, $\theta_3 = 249.21°$, and a peak of 4.1σ above the mean, and subsequent translation function components $T_x = 34.55$, $T_y = 21.90$, $T_z = 24.28$ Å, and a correlation coefficient of 0.52. Rigid-body refinement at 20.0–2.6 Å resolution resulted in an initial R_{work} of 0.38. The K64H-R67N HCA III data were isomorphous with the K64H HCA III data (Table I) and this allowed the use of the refined K64H HCA III model as a phasing model. Rigid-body refinement at 20.0–2.5 Å resolution yielded in an initial R_{work} of 0.34.

All structures were refined using standard protocols within the software package CNS.[25] The $2F_0 - F_c$ and $F_0 - F_c$ Fourier maps were generated after one cycle of rigid body refinement, annealing by heating to 3000 K with gradual cooling, geometry-restrained position refinement, and temperature factor refinement. The maps were visually inspected using the program O version 7[26] and each clearly showed the position of the zinc and the mutated residues, which were subsequently built into the respective electron density maps. After several cycles of refinement, solvent molecules were incorporated into the models using the automatic water-picking program in CNS until no more water molecules were found at a 2.0σ level. Refinement of the models continued until convergence of the R_{work} and R_{free} was reached. Ramachandran statistics for the structural models were calculated using the program *PROCHECK*[27] and resulted in standard values for the percentage of dihedral angles in the most favored, additional and generously allowed regions. A summary of the refinement and final model statistics for K64H, R67H, and K64H-R67N HCA III are given in Table I and the atomic coordinates have been deposited with the Protein Data Bank (entries 2HFX, 2HFY, and 2HFW, respectively).

RESULTS

Crystallography

Crystal structures were obtained for three site-specific mutants of HCA III: K64H, R67H, and the double-mutant K64H-R67N. Each final, refined model had acceptable geometries and could be superposed onto the structure of wild type HCA III with a root mean square deviation of <1 Å for all C_αs (Protein Data Bank entry 1Z93).

Comparison of the active sites showed that the side chain of His64 in K64H HCA III had the same overall orientation as Lys64 in wild type HCA III.[3,28] Inspection of the K64H HCA III structure indicated a single conformation of the imidazole side chain of His64 located about 12 Å from the zinc (Fig. 2). This side chain had an average B-factor of ~14 Å^2, implying that this orientation is well-ordered when compared with the average side-chain B-factor of ~16 Å^2 (Table I). Another feature of His64 in K64H HCA III is the close proximity of its imidazole side chain to the indole ring of Trp5, a distance of 3.5 Å between the aromatic rings that is consistent with a π-stacking interaction (Fig. 2). Interestingly, this orientation is similar to the outward orientation observed for His64 in HCA II structures (Table II; Fig. 1).[4,29] A similar π-stacking interaction has been reported between 4-methylimidazole, an activator of catalysis, and the indole ring of Trp 5 in H64A HCA II.[15,30]

TABLE II. Comparison of Side-Chain Torsion Angles of His64 and His67 in the Outward Conformations in HCA II and HCA III and Mutants

Enzyme	Crystallization pH	Torsion angles (°) χ_1	χ_2
K64H HCA III	5.8	−59	−66
R67H HCA III	5.8	−88	−124
K64H-R67N HCA III	5.8	−51	−71
T200S HCA II[a]	8.0	−50	−68
Wild-type HCAII[b]	7.8	−42	−88

[a]Data from Krebs et al.[34] PDB accession code: 5CA2.
[b]Data from Fisher et al.[4] PDB accession code: 1TBT.

To test the hypothesis that the orientation of the side chain of His64 is influenced by the nearby Arg67, we examined the double mutant K64H-R67N HCA III. The crystal structure showed His64 in K64H-R67N HCA III occupying the same position as His64 in the outward position of HCA II (Fig. 2, Table II). Asn67 in K64H-R67N HCA III superposes very well with Asn67 in HCA II. The side chain of His64 in K64H-R67N HCA III exhibits the same π-stacking interaction with Trp5 as observed for His64 in K64H HCA III. However, His64 in the double mutant is less well ordered compared with His64 in K64H HCA III, with an average B-factor of ~33 Å^2 compared with ~39 Å^2 for all side chains (Table I).

In contrast, the structure of R67H HCA III showed the side chain of His67 extending into the active-site cavity in a single orientation with the imidazole ring ~7 Å from the zinc ion (Table II; Fig. 2). This is different than Arg67 in wild type HCA III,[3] which has its side chain oriented away from the zinc, towards the opening of the active-site cavity (Fig. 1). Unlike His64 in K64H HCA III, the side chain of His67 in R67H HCA III was less well ordered with an average B-factor of ~30 Å^2, compared to the average side-chain B-factor of ~24 Å^2 (Table I). The side chain of K64 in R67H HCA III was shifted slightly compared to its orientation in wild type HCA III and appeared closer to the zinc by ~1 Å (Figs. 1 and 2). This is probably due to the properties of His67 that do not exert the same electrostatic repulsion as an Arg at that position.

Inspection of the active site structure of K64H HCAIII showed that a plausible water network can be formed between the zinc-bound solvent and side chain of His64. However, an accurate comparison of the solvation states in the other mutants is not possible due to the differences in the resolution and number of solvent molecules built in each structure (Table I).

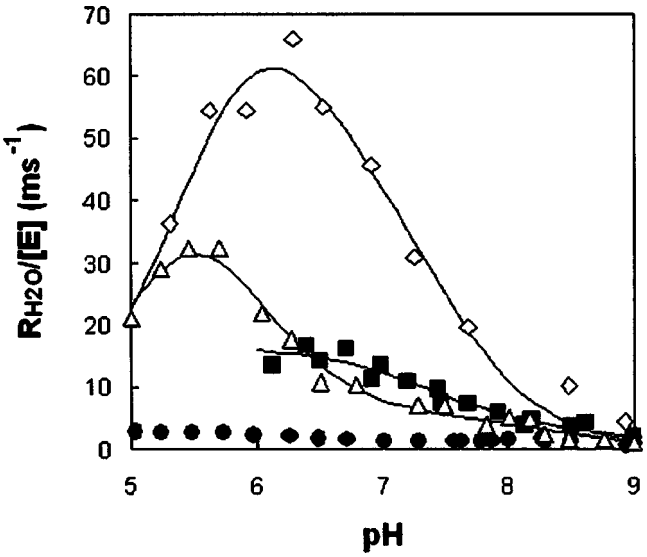

Fig. 3. The pH profile of R_{H2O}/[E], the rate constant for release from enzyme of ^{18}O-labeled water during catalysis, for (filled square) K64H HCA III, (open diamond) K64H-R67N HCA III, (open triangle) R67H HCA III, and (filled circle) wild-type HCA III. Solutions contained 25–100 m*M* total concentration of all species of CO_2 with total ionic strength maintained at 0.2 *M* by addition of sodium sulfate. No buffers were added and temperature was 25°C. The solid lines are fits (Enzfitter, Biosoft) of Eq. (5) to the data with parameters given in Table III. Data for K64H and K64H-R67N HCA III from Jewel et al.[11] for R67H from Ren et al.[31] Data for HCA III over a smaller pH range were determined by Jewel et al.[11]

TABLE III. Maximal, pH Independent Values of Rate Constants k_B for Proton Transfer from Proton Donors (His64 or His67) to the Zinc-Bound Hydroxide in Variants of HCA II and HCA III Determined by Catalyzed Rates of ^{18}O Exchange Between CO_2 and Water

Enzyme	k_B (ms^{-1})[a]	$(pK_a)_{His}$[a]	$(pK_a)_{ZnH_2O}$[a]
Wild-type HCA II	800	7.2	6.9
Variants of HCA III			
Wild-type	3.0	—[c]	<6
K64H[b]	20	7.5	<6
K64H-R67N[b]	100	7.5	5.3
R67H[d]	81	5.6	5.3
K64A-R67H[d]	59	6.2	6.0

[a]The standard errors in k_B were ±20% or less. Standard errors in pK_a were ±0.2 or less, except for wild-type and K64H HCA III for which an upper limit is given for the pK_a of the donor. Since there is no pH dependence of R_{H_2O} for wild-type HCA III, the value of k_B is taken as R_{H_2O}/[E]. This is consistent with a model in which $(pK_a)_{His}$ and $(pK_a)_{ZnH_2O}$ of Eq. (5) are outside the pH range of these measurements. The values of k_B and $(pK_a)_{His}$ for K64H HCA III were determined from Eq. (5) assuming $[H^+]/(K_a)_{ZnH_2O} \ll 1$.
[b]From Silverman et al.[22]
[c]HCA III has Lys64 and there is no His acting as proton shuttle.
[d]From Ren et al.[31]

Catalysis

In this study we emphasize the proton transfer that is the rate-limiting step in RH2O/[E], a rate constant for the release from the enzyme of $H_2{}^{18}O$, as shown in Eqs. (4) and (5). These ^{18}O-exchange experiments were carried out at chemical equilibrium in the absence of added buffers, an experiment in which proton transfer in the catalysis is predominantly intramolecular. The pH profiles for R_{H_2O}/[E] can be described by the transfer of a single proton from a proton donor residue in the active site to the zinc-bound hydroxide in the dehydration direction [Eq. (4)]. Fitting Eq. (5) to data in Figure 3 (Enzfitter, Biosoft) gave estimates of the pK_a of the proton donor and acceptor as well as the rate constant k_B for the proton transfer [Eq. (5); Table III].[21,22]

Each of the mutants of HCA III studied here has a histidine placed in the active-site cavity at position 64 (as in HCA II) or at position 67 (as in HCA I), and in each case there is a substantial increase in proton transfer in catalysis as measured by k_B (Fig. 3, Table III). This increase is attributed to enhanced proton transfer consistent with the pH profiles in which the expected pK_a (near pK_a 7) of a histidine residue is found. The rate constants k_B for proton transfer during catalysis are appreciably smaller for the mutants and wild-type HCA III compared with wild-type HCA II (Fig. 3; Table III), as noted previously.[11,22,31] The pH profiles for R67H and K64H-R67N HCA III are bell-shaped and give values of k_B and the pK_a of donor and acceptor groups (Fig. 3). For K64H HCA III in Figure 3, the value of ^kB [Eq. (5)] is described by a single ionization consistent with His64 acting as a proton donor with pK_a 7.5 ± 0.2 and a maximum near 20 ms^{-1}. An upper limit for the value of the pK_a of the zinc-bound water in K64H HCA III was determined from the pH profile of k_{cat}/K_m and is given in Table III (see also Ref. 11). In the case of R67H and K64A-R67H HCA III, the pK_a obtained from pH profiles for His67 is near 6, consistent with the ^1H NMR titration of His67 in HCA I (Campbell et al., 1974).[32] Further evidence supports the predominant role of proton transfer in k_B, specifically chemical rescue by imidazole[11] and isotope effects in mutants of HCA III containing His64[22] and His67,[31] although these are not the specific mutants of Table I.

DISCUSSION

HCA III has a low catalytic activity (3 ms^{-1}; Table III) compared with HCA II (800 ms^{-1}), in part because it lacks the proton shuttle residue His64. Here we have replaced with histidine two residues located in the active-site cavity of HCA III, Lys64 and Arg67, and compared structure and proton transfer efficiency to elucidate how differences in the molecular environment affect proton transfer rates. In previous crystallographic studies of HCA II, the side chain of His64 has been shown to have two distinct conformational orientations with populations depending somewhat on the pH of crystallization. One is an inward conformation (predominant especially at > pH 8) with the imidazole side chain of His64 pointing towards the zinc ion, and the other an outward conformation (present at pH 6–9) with the side chain pointing towards the opening of the active-site cavity (Fig. 1).[4,27,33]

There is a strong argument that an efficient proton transfer residue in carbonic anhydrase requires side-chain mobility, perhaps to span the proton transport distance from the zinc to bulk solvent in a conical shaped cavity 15 Å deep. Mobility of the side chain of His64 is suggested by its two observed conformations in the structure of wild type HCA II.[4,29] Additional support for the idea of a mobile proton shuttle group is the result with CA V in which a chemically modified cysteine provides a mobile shuttle,[34] and with the γ-carbonic anhydrase of *Methosarcina thermophila* in which the proton shuttle residue is Glu84,[35] in both cases multiple side-chain conformations of the shuttle residue are observed in the crystal structures.

In the structure of K64H HCA III, the side chain of His64 appears only in one conformation (see Fig. 2) with dihedral angles similar to His64 in the outward conformation of HCA II and also similar to His64 in T200S HCA II (Table II).[36] An outward conformation at pH 8.0 was observed for the mutant T200S HCA II;[36] this mutant had catalytic activity very close to wild type, suggesting that in this mutant the orientation of His64 observed in the crystal structure may not be relevant to catalysis. Although there is good evidence from the pH profile (Fig. 3), chemical rescue,[11] and solvent H/D isotope effects[22] that His64 in K64H HCA III is a proton shuttle residue, its efficiency in proton transfer measured by the maximal, pH-independent rate constant k_B is only 2.5% that of HCA II (Table III). Comparison of crystal structures suggests that this difference is due, at least in part, to the restricted outward side-chain conformation of His64 in K64H HCA III compared with that in HCA II (Figs. 1 and 2). Observation of only an outward conformation for His64 in K64H HCA II suggests a restricted mobility that may limit the transfer of protons during catalysis; moreover, this outward conformation, without an appreciable population in the inward orientation, may be too distant to donate or accept a proton from the zinc-bound solvent. This is consistent with the conclusion of An et al.[17] that 4-methylimidazole bound in a π-stacking or cationic interaction with the indole ring of the side chain of Trp5 approximates the position of His64 in the outward orientation and does not transfer protons in catalysis. That study concluded that an outward conformation of His64 is not efficient in proton transfer. We suggest that this same feature limits proton transfer in K64H HCA III. Hence, the absence of His64 in HCA III by itself does not account for the low catalytic activity of this mutant. Other residues in the active-site cavity of HCA III, such as Phe198 discussed later, may also cause its low catalytic activity and perhaps contribute to the inefficiency of His64 as a proton shuttle in K64H HCA III.

At the pH of crystallization of K64H HCA III (pH 5.8) the side chain of His64 (pK_a 7.5, Table III) should be predominantly protonated and charged. However, the outward orientation of His64 in K64H HCA III is not due to an electrostatic repulsion between the positively charged side chains of His64 and Arg67, since the crystal structure of K64H-R67N HCA III also has His64 in the outward orientation (Fig. 2). However, k_B the maximal rate constant for proton transfer is greater by fivefold for K64H-R67N compared with K64H HCA III (Table III). Clearly the replacement of Arg67 with Asn has improved catalytic efficiency, and the crystallographic data indicate that this has happened with no apparent change in the conformation of His64 in the crystal structure. Other sources promoting proton transfer efficiency must be responsible including possible changes in solvation in the active site or side chain conformations for His64 not apparent in the crystal structure. Another feature of the active site of HCA III that is likely involved in influencing proton transfer is Phe198, which is unique to this isozyme. This residue is Leu in HCA II and most other carbonic anhydrases in the α-class.[37] Earlier reports of HCA III, both of catalysis[15] and crystal structure,[3] confirm that the replacement of Phe198 with Leu gives properties to F198L HCA III that make it more like HCA II. The role of Phe198 in the preferred outward orientation of His64 in mutants of HCA III is yet to be determined.

The crystal structure of R67H HCA III suggests that the enhancement of proton transfer by this mutant (Table III) is related to the prominent orientation of the His67 side chain in the active-site cavity near the zinc (Fig. 2). The side chain of His67 in R67H HCA III extends into the active-site cavity exhibiting a somewhat inward orientation (Table II; Fig. 2). In R67H HCA III the side chain of His67 is about as close to the zinc as is His64 in the inward orientation in HCA II (7–8 Å); its efficiency in proton transfer is fourfold greater than that for K64H HCA III but just 10% that of HCA II (Table III). No alternate side-chain conformations were observed for His67. This lower efficiency of proton transfer in R67H HCA III compared with HCA II may reflect the lack of side chain mobility of His67 or simply a side-chain orientation that precludes formation of a hydrogen-bonded network efficient for proton transfer. There appears little effect of Lys64 on the proton transfer capacity of His67 in R67H HCA III; the mutant K64A-R67H has approximately the same value of k_B as does R67H HCA III (Table III).

In summary, these data show an association between low activity in variants of carbonic anhydrase III and an outward orientation of His64 in the crystal structure. This study suggests that residues in the active site cavity of the efficient carbonic anhydrases function, in part, to promote conformations and mobility of His64 that promote proton transfer. The question of the function of the highly conserved residues Lys64 and Arg67 in CA III still remains unanswered. This issue extends to the overall differences between the active site of HCA III and other isozymes of animal and human carbonic anhydrase, including a more constricted active-site cavity containing an accumulation of basic residues in HCA III. It is likely that the function of these basic residues in CA III will be more evident if a physiological role for this isozyme can be determined.[38]

ACKNOWLEDGMENTS

We are pleased to acknowledge the assistance of Lakshmanan Govindasamy and Robbie Reutzel in the crystallographic analysis.

REFERENCES

1. Tu CK, Sanyal G, Wynns GC, Silverman DN. The pH dependence of the hydration of CO_2 catalyzed by carbonic anhydrase III from skeletal muscle of the cat: steady state and equilibrium studies. J Biol Chem 1983;258:8867–8871.
2. Khalifah RG. The carbon dioxide hydration activity of carbonic anhydrase. J Biol Chem 1971;246:2561–2573.
3. Duda DM, Tu CK, Fisher Z, An H, Yoshioka C, Govindasamy L, Laipis PJ, Agbandje-McKenna M, Silverman DN, McKenna R. Human carbonic anhydrase. III. Structural and kinetic study of catalysis and proton transfer. Biochemistry 2005;44:10046–10053.
4. Fisher SZ, Hernandez J, Tu CK, Duda D, Yoshioka C, An H, Govindasamy L, Silverman DN, McKenna R. Structural and kinetic characterization of active-site histidine in catalysis by carbonic anhydrase II. Biochemistry 2005;44:1097–1105.
5. Eriksson EA, Liljas A. Refined structure of bovine carbonic anhydrase III at 2.0 A resolution. Proteins: Struct Funct Genet 1993;16:29–42.
6. Lindskog S. Structure and mechanism of carbonic anhydrase. Pharmacol Ther 1997;74:1–20.
7. Northrop DB, Rebholz KL. Kinetics of enzymes with iso-mechanisms: solvent isotope effects. Arch Biochem Biophys 1997;342:317–321.
8. Steiner H, Jonsson BH, Lindskog S. The catalytic mechanism of carbonic anhydrase. Hydrogen-isotope effects on the kinetic parameters of the human C isoenzyme. Eur J Biochem 1975;59:253–259.
9. Tu CK, Silverman DN, Forsman C, Jonsson BH, Lindskog S. Role of histidine 64 in the catalytic mechanism of human carbonic anhydrase II studied with a site-specific mutant. Biochemistry 1989;28:7913–7918.
10. Christianson DW, Fierke CA. Carbonic anhydrase: evolution of the zinc binding site by nature and by design. Acc Chem Res 1996;29:331–339.
11. Jewell DA, Tu CK, Paranawithana SR, Tanhauser SM, LoGrasso PV, Laipis PJ, Silverman DN. Enhancement of the catalytic properties of human carbonic anhydrase III by site-directed mutagenesis. Biochemistry 1991;30:1484–1490.
12. Esnouf RM. An extensively modified version of MolScript that includes greatly enhanced coloring capabilities. J Mol Graph Model 1997;15:132–134,112–113.
13. Merritt EA, Bacon DJ. Raster3D Version 2: photorealistic molecular graphics. Methods Enzymol 1997;277:505–524.
14. Mallis RJ, Poland BW, Chatterjee TK, Fisher RA, Darmawan S, Honzatko RB, Thomas JA. Crystal structure of *S*-glutathiolated carbonic anhydrase III. FEBS Lett 2000;482:237–241.
15. LoGrasso PV, Tu CK, Chen X, Taoka S, Laipis PJ, Silverman DN. Influence of amino-acid replacement at position 198 on catalytic properties of zinc-bound water in human carbonic anhydrase III. Biochemistry 1993;32:5786–5791.
16. Tu CK, Chen X, Ren X, LoGrasso PV, Jewell DA, Laipis PJ, Silverman DN. Interactions of active-site residue and catalytic activity of human carbonic anhydrase III. J Biol Chem 1994;269:23002–23006.
17. An H, Tu CK, Duda D, Montanez-Clemente I, Math K, Laipis PJ, McKenna R, Silverman DN. Chemical rescue in catalysis by human carbonic anhydrases II and III. Biochemistry 2002;41:3235–3242.
18. Tannhauser SM, Jewell DA, Tu C, Silverman DN, Laipis PJ. A T7 vector optimizeed for site-directed mutagenesis using oligodeoxyribonucleotide cassettes. Gene 1992;117:113–117.
19. Studier FW, Rosenberg AH, Dunn JJ, Dubendorf JW. .Use of T7 RNA polymerase to direct expression of cloned genes. Methods Enzymol 1990;185:60–89.
20. Tu CK, Thomas HG, Wynns GC, Silverman DN. Hydrolysis of 4-nitrophenyl acetate catalyzed by carbonic anhydrase III from bovine skeletal muscle. J Biol Chem 1986;261:10100–10103.
21. Silverman DN. Carbonic anhydrase: oxygen-18 exchange catalyzed by an enzyme with rate-contributing proton-transfer steps. Methods Enzymol 1982;87:732–752.
22. Silverman DN, Tu C, Chen X, Tanhauser SM, Kresge AJ, Laipis PJ. Rate-equilibria relationships in intramolecular proton transfer in human carbonic anhydrase III. Biochemistry 1993;32:10757–10762.
23. McPherson A. Preparation and analysis of protein crystals. New York: Wiley; 1982.
24. Otwinoski Z, Minor W. Processing of X-ray diffraction data collected in oscillation mode. Methods Enzymol 1997;276:307–326.
25. Brunger AT, Adams PD, Core GM, Delano WL, Gross P, Grosse-Kunstleve RW, Jiang JS, Kuszewski J, Nilges N, Pannu NS, Read RJ, Rice LM, Simonson T, Warren GL. Crystallography and NMR system: a new software suite for macromolecular structure determination. Acta Crystallogr D 1998;54:905–921.
26. Jones TA, Zou JY, Cowan SW, Kjeldgaard M. Improved methods for building protein models in electron density maps and the location of errors in these models. Acta Crystallogr 1991;47:110–119.
27. Laskowski RA, MacArthur MW, Moss DS, Thornton JM. PROCHECK—a program to check the stereochemical quality of protein structures. J Appl Cryst 1993;26:283–291.
28. Duda DM, Yoshioka C, Lakshmanan G, An H, Tu CK, Silverman DN, McKenna R. Crystallization and preliminary X-ray analysis of human carbonic anhydrase III. Acta Crystallogr D 2002;58:849–852.
29. Nair SK, Christianson DW. Unexpected pH-dependent conformation of His64, proton shuttle of carbonic anhydrase II. J Am Chem Soc 1991;113:9455–9458.
30. Duda D, Tu CK, Qian M, Laipis P, Agbandje-McKenna M, Silverman DN, McKenna R. Structural and kinetic analysis of the chemical rescue of the proton transfer function of carbonic anhydrase II. Biochemistry 2001;40:1741–1748.
31. Ren X, Tu CK, Laipis PJ, Silverman DN. Proton transfer by Histidine 67 in site-directed mutants of human carbonic anhydrase III. Biochemistry 1995;34:8492–8498.
32. Campbell ID, Lindskog S, White AI. Study of histidine residues of human carbonic anhydrase-B using 270 MHz proton magnetic resonance. J Mol Biol 1974;90:469–489.
33. Håkansson K, Wehnert A. Structure of cobalt carbonic anhydrase complexed with bicarbonate. J Mol Biol 1992;228:1212–1218.
34. Jude KM, Wright SK, Tu C, Silverman DN, Viola RE, Christianson DW. Crystal structure of F65A/Y131C-methylimidazole carbonic anhydrase V reveals architectural features of an engineered proton shuttle. Biochemistry 2000;41:2485–2491.
35. Iverson TM, Alber BE, Kisker C, Ferry JG Rees DC. A closer look at the active site of γ-class carbonic anhydrases: high-resolution crystallographic studies of the carbonic anhydrase from Methanosarcina thermophila. Biochemistry 2000;39:9222–9231.
36. Krebs JF, Fierke CA, Alexander RS, Christianson DW. Conformational mobility of His-64 in the Thr-200→Ser mutant of human carbonic anhydrase II. Biochemistry 1991;30:9153–9160.
37. Hewett-Emmett D, Tashian RE. Functional diversity, conservation, and convergence in the evolution of the α-, β-, and γ-carbonic anhydrase gene families. Mol Phylogenet Evol 1996;5:50–77.
38. Kim G, Lee T, Wetzel P, Geers C, Robinson MA, Myers TG, Owens JW, Wehr NB, Eckhaus MW, Gros G, Wynshaw-Boris A, Levine RL. Carbonic anhydrase III is not required in the mouse for normal growth, development, and life span. Molec Cell Biol 2004;24:9942–9947.